EUV Analysis of a Multi-Threaded Prominence

V. Jerčić, R. Keppens

Centre for mathematical Plasma Astrophysics, Department of Mathematics, KU Leuven, Leuven, Belgium

Abstract We perform a realistic, 2D simulation where a prominence with fine structure is formed as a consequence of thermal instability. From it, we synthesize extreme ultraviolet (EUV) and Hα images. We find that the synthesized images share similar characteristics to the real observational ones.

Introduction Prominences are plasma structures found within the solar corona, the outermost layer of the Sun's atmosphere. On the smallest scales resolvable with observations we find they are made of numerous smaller structures, the so-called prominence fibrils or threads. Unlike the large scale prominence, threads have a life time of a few to about 20 min and exhibit multi-directional, counter-streaming motion. The exact origin of these fine structures and their constant motion is still unclear. A prominence observed at different wavelengths corresponds to different temperatures, revealing its multi-thermal structure. Hα and Ca II bands are chromospheric lines that sample the coolest temperatures *i.e.*, thread's core regions. He II 304 Å, Fe VIII 131 Å, Fe IX 171 Å (extreme ultraviolet, EUV lines) are transition region lines that sample the properties of the prominence-corona transition region (PCTR). However, the fact that one in essence obtains line-of-sight integrated information, even for optically thin lines makes these observational data difficult to interpret. Hence, analyzing the synthetic images of a simulation from which we know the "ground-truth" can lead to better comprehension of the real observations.

Methods The magnetohydrodynamic (MHD) equations (1)-(4) with non-adiabatic effects included, were solved using the open-source MPI Adaptive Mesh Refinement Versatile Advection Code (MPI-AMRVAC[1]) [1]. We simulate a 2D magnetic arcade (Fig. 1) 150 Mm in length and 8 Mm in width following the geometrical prescription as in [2]. The only difference being that the central dip section is now 8 Mm deep. The function $\Lambda(T)$ represents radiative loss per unit mass and is prescribed

$$\frac{\partial \rho}{\partial t} + \nabla \cdot (\rho \mathbf{v}) = 0 \tag{1}$$

$$\frac{\partial \rho \mathbf{v}}{\partial t} + \nabla \cdot \left(\rho \mathbf{v}\mathbf{v} + p_{tot}\mathbf{I} - \frac{\mathbf{B}\mathbf{B}}{\mu_0} \right) = \rho \mathbf{g} \tag{2}$$

$$\frac{\partial e}{\partial t} + \nabla \cdot \left(e\mathbf{v} - \frac{\mathbf{B}\mathbf{B}}{\mu_0} \cdot \mathbf{v} + \mathbf{v} p_{tot} \right) = \rho \mathbf{g} \cdot \mathbf{v} + \nabla \cdot (\kappa \cdot \nabla T) - n_H n_e \Lambda(T) + H \tag{3}$$

$$\frac{\partial \mathbf{B}}{\partial t} + \nabla \cdot (\mathbf{v}\mathbf{B} - \mathbf{B}\mathbf{v}) = 0 \tag{4}$$

[1] http://amrvac.org/

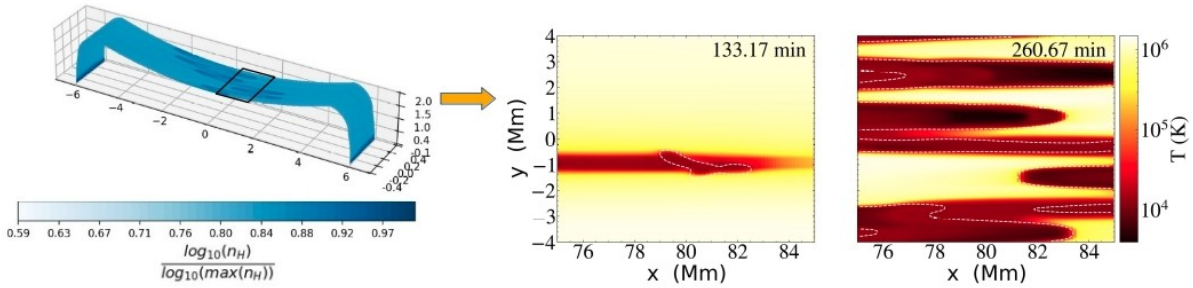

Figure 1: On the left is the 3D representation of our domain with over-plotted, normalized number density values at $t = 261$ min. The two panels on the right show the temperature distribution cut-out (black square) at $t = 133$ min and 261 min with contour lines ($n_H > 7 \times 10^9$ cm^{-3}) marking the threads.

with a cooling curve [3]. H represents heating that is a sum of steady background heating and a localized (in time and space) random heating. Background heating is needed to maintain the hot corona and is simulated as a simple exponential function that decays along the footpoints of the magnetic arcade. It has a scale length of $L_x/2$, where L_x marks the full length of the domain in the x direction (150 Mm) and an amplitude of $E_0 = 5 \times 10^{-5}$ erg cm^{-3} s^{-1}. We created the localized heating on the basis of the heating function used in [4] that we modified for a 2D setup. We perform a relaxation phase of about 50 min, after which we start with the localized heating. To properly solve the described set of equations we employ a Harten-Lax-van Leer (HLL) approximate Riemann solver for the spatial discretisation, combined with a third order, asymmetric shock-capturing slope limiter. The courant number we used is 0.8. Five-step (strong stability preserving) fourth-order Runge-Kutta method is used for the time discretisation. To maintain the divergence of the magnetic field at machine precision zero for a prechosen discrete evaluation, we use the upwind constrained transport method. We employ adaptive grid refinement, where we use a density threshold as a condition to refine. We use two levels of refinement (including the base level), with 520×100 cells on the base level (144 km$\times$40 km on the highest level of refinement). Along the transfield y direction we use periodic boundary conditions. Along the field-aligned x direction at the footpoints, the magnetic field is extrapolated, the velocity is reflective and the pressure and density are fixed according to the values calculated from the hydrostatic equilibrium. In order to make a comparison of our simulated domain with real data, we made synthetic EUV images (in 304, 171, and 211 Å) using AMRVAC. The primitive density and temperature variables are converted to intensity. The local emission intensity for each wavelength is calculated as $n_e^2 G(n_e, T)$, where G represents the contribution function obtained from the CHIANTI[2] database [5]. We have a cut-off emissivity value at a negligibly small value

[2] `https://www.chiantidatabase.org/`

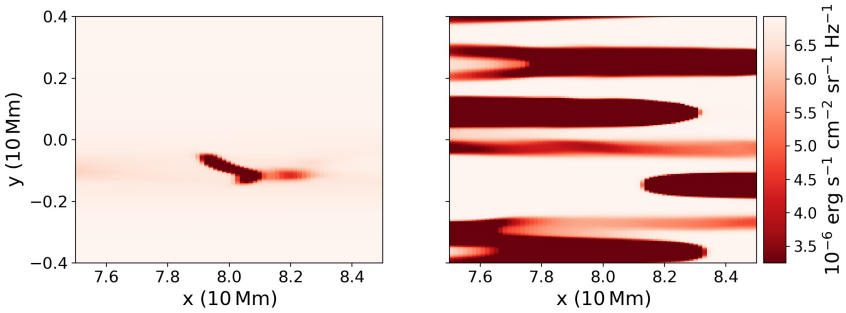

Figure 2: Same part of the domain as on Fig. 1 showing the Hα at $t = 133$ min and 261 min.

of 10^{-12} DN cm^{-1} s^{-1} px^{-1}. The Hα figures were calculated according to the approximate fast radiative transfer method [6], using the implementation in [7].

Results and Conclusion Figure 1 shows the temperature distribution in the domain, where the white, dashed contour lines represent the number density threshold ($n_H > 7 \times 10^9$ cm^{-3}) used to define the prominence plasma. On the left panel (133 min after the localized heating was turned on), the orange to reddish "cold" region surrounds the newly formed thread at temperatures of $\sim$0.08 MK, while the thread itself (inside the contour line) has an average temperature of $\sim$0.04 MK. The right panel shows $t = 260.67$ min, when the threads already have an average temperature of $\sim$0.011 MK. Figure 2 shows the Hα representation of Fig. 1. We can easily notice the similarities of the Hα representation in comparison to the contour lines in Fig. 1. The corresponding EUV images are presented in Fig. 3 (left panels for $t = 133$ min and right ones for $t = 261$ min). Such images are made using broadband filters that integrate across several Å. As a consequence, the measured intensity is sourced from more than a single element, complicating the interpretation of the bright and dark regions in the images. The same is also the case with our synthetic images. However, the structural variations in intensity come from a single layer (1 Mm thick) whose temperature and density distribution we know exactly. Hence we can make a one-to-one connection between the combination of temperatures and densities and the subsequent emission. Furthermore, our synthetic images contain no background radiation that, although operationally important, further complicates the analysis. In the top left panel of Fig. 3 we see in the 171 Å that the dark, cold area where the density peaks and the temperature drops (initial thread structure) is surrounded by a wide, bright band. As the temperature around the thread is relatively uniform at that moment, and at $\sim$0.8 MK, the 171 Å intensity is high. The bottom left panel of Fig. 3, in 304 Å, shows the brightest layer around the forming thread, it corresponds to a region of temperature of about 0.08 MK. The cospatial peaked gradient emission is indicative of the PCTR. However, those bright regions show an unusually extended area around the location the thread actually forms. This is a

consequence of neglecting the background illumination and associated photoionisation that would otherwise populate this void with varying intensity depending on the local optical thickness.

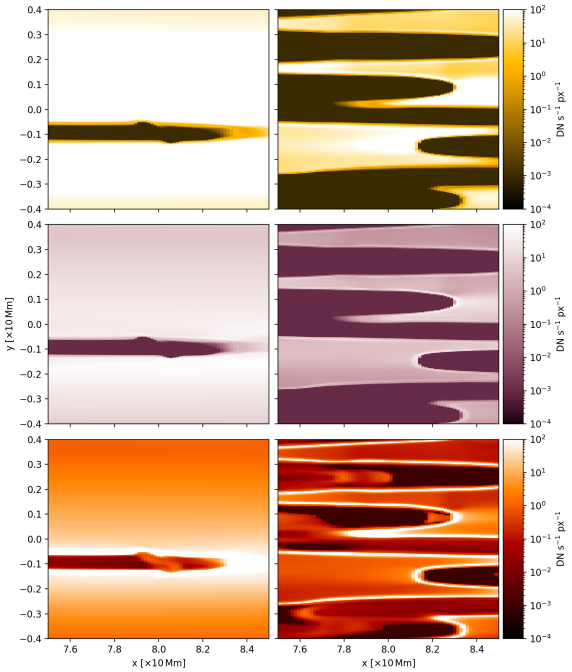

Figure 3: Synthetic EUV emission in 171 Å, 211 Å and 304 Å (top, middle and bottom panels, respectively). The left panels are at $t = 133$ min and the right ones at $t = 261$ min.

The real area of the thread is much more clearly seen in the Hα images (Fig. 2). The right panels of Fig. 3 show how the EUV images change as the realistic threads form. The extent of the bright region in 171 Å significantly decreased, and is now considerably thinner. Emission at 211 Å are typically related to temperatures close to 2 MK that are not found in the region shown here. However, as the temperature response of 211 Å is not singly peaked, we notice that the 211 Å shows emission at temperatures of $\sim$1 MK. Once again, the 304 Å emission in the bottom right panel shows the most detail and also delineates clearly the edge of the threads (PCTR). At this point, we find this layer to be somewhat thinner and closer to the real thread boundary (cf. Fig. 2) than during the formation.

Conclusion The EUV images, synthesized from the described simulation, show characteristics similar to what we see from observations. During the initial stage of the thread formation, the EUV images deviate more from the Hα representation, with the differences decreasing at later stages. As we we have only local emissivity-based representations in the EUV lines, an improvement is possible by taking into account the background radiation. Moreover, we approximate the plasma as optically thin. Even though a good approximation for the hotter Fe lines, the He I 304 Å is already affected by prominence optically thick-properties.

References

[1] C. Xia, J. Teunissen, I. El Mellah, E. Chané, and R. Keppens, *ApJS*, **234** (2018)

[2] Jerčić, V., Keppens, R., and Zhou, Y., *A&A* **658**, (2022)

[3] Schure, K. M., Kosenko, D., Kaastra, J. S., Keppens, R., and Vink, J., *A&A*, **508** (2009)

[4] Antolin, P., Shibata, K., and Vissers, G.: *ApJ* **716** (2010).

[5] Del Zanna, G., Dere, K. P., Young, P. R., Landi, E., and Mason, H. E.,*A&A*, **582** (2015)

[6] Heinzel, P., Gunár, S., and Anzer, U., *A&A* **579**, (2015)

[7] Claes, N., Keppens, R., and Xia, C., *A&A*, **636** (2020)